IEEE Transactions on Quantum Engineering

Received 25 December 2022; revised 11 March 2023; accepted 28 March 2023; date of publication 18 April 2023; date of current version 31 May 2023.

Digital Object Identifier 10.1109/TQE.2023.3266946

Millimeter-Waves to Terahertz SISO and MIMO Continuous Variable Quantum Key Distribution

MINGQI ZHANG[1], STEFANO PIRANDOLA[2], AND KAVEH DELFANAZARI[1]

[1]Electronics and Nanoscale Engineering Division, James Watt School of Engineering, University of Glasgow, G12 8QQ Glasgow, U.K.

[2]Department of Computer Science, University of York, YO10 5GH York, U.K.

Corresponding author: Kaveh Delfanazari (e-mail: kaveh.delfanazari@glasgow.ac.uk).

The work of K. Delfanazari was supported in part by the Royal Society Research under Grant RGS/R2/222168 and in part by the Research Fellowship from the Royal Society of Edinburgh, and the work of S. Pirandola supported in part by the EPSRC via the Quantum Communications Hub under Grant EP/T001011/1 and in part by the EU via QUARTET under Grant 862644.

ABSTRACT With the exponentially increased demands for large bandwidth, it is important to think about the best network platform as well as the security and privacy of the information in communication networks. Millimeter (mm)-waves and terahertz (THz) with high carrier frequencies are proposed as the enabling technologies to overcome Shannon's channel capacity limit of existing communication systems by providing ultrawide bandwidth signals. Mm-waves and THz are also able to build wireless links compatible with optical communication systems. However, most solid-state components that can operate reasonably efficiently at these frequency ranges (100 GHz–10 THz), especially sources and detectors, require cryogenic cooling, as is a requirement for most quantum systems. Here, we show that secure mm-waves and THz quantum key distribution (QKD) can be achieved when the sources and detectors operate at cryogenic temperatures down to $T = 4$ K. We compare single-input single-output and multiple-input multiple-output (MIMO) continuous variable THz quantum key distribution (CVQKD) schemes and find the positive secret key rate in the frequency ranges between $f = 100$ GHz and 1 THz. Moreover, we find that the maximum transmission distance could be extended, the secret key rate could be improved in lower temperatures, and achieve a maximum secret communication distance of more than 5 km at $f = 100$ GHz and $T = 4$ K by using 1024×1024 antennas. Our results for the first time show the possibility of mm-waves and THz MIMO CVQKD with the system operating at temperatures below $T = 50$ K, which may contribute to the efforts to develop next-generation secure wireless communication systems and quantum internet for applications from intersatellite and deep space to indoor and short-distance communications.

INDEX TERMS 6G communication, cryogenic system, cryptography, millimeter (mm)-waves, multiple-input multiple-output (MIMO), quantum communication, quantum key distribution (QKD), single-input single-output (SISO), terahertz (THz) waves.

I. INTRODUCTION

With the extension of wireless communication and the fast development of information security, higher carrier frequencies and more spectral resources are required [1], [2]. Millimeter (mm)- and terahertz (THz)-waves [3], [4], [5], [6] offer ultrawide bandwidth and high-speed data rate communication and are considered to build next-generation (6G) communication systems [7], [8], [9], [10], [11]. Mm-waves and THz bands lie between the mature microwave and optical bands as less explored areas [12], [13], [14], [15], [16]. A gap in the electromagnetic (EM) spectrum exists at these frequency ranges due to the inefficient and unpractical devices and circuits [1], [2], [3], [4], [5], [6], [7], [8], [9], [10], [11], [12], [13], [14], [15]. [16], [17], [18], [19]. However, the recent development of electronic, photonic, and plasmonic-based mm-waves and THz technologies help close this gap with the demonstration of power-efficient sources [20], [21], [22], [23], [24], [25], [26], antennas [27], [28], [29], [30], [31], filters [32], [33], [34], waveguides [29], [35], [36], [37], [38], [39], modulators [40], [41], [42], [43], [44], [45], [46], [47], [48], [49], and detectors [3], [49], [50], [51], [52]. Demands for 6G are including, but are not limited

to, Terabit per second, mm-precision sensing and positioning, seamless connectivity, and ultrafast wireless communications [7], [8], [9], [10], [11]. Moreover, practical implementation of quantum processors and quantum computers operating at low temperatures (cryogenics) [53], [54], [55] requires massive open air and free space data transfer from and to high-performance classical processors, computers, and communication systems. Therefore, to realize a robust building block for practical quantum information, processing attention should be on both security and low-temperature operation. EM waves traveling through the free space channel will get impacted by several atmospheric effects, such as atmospheric attenuation caused by absorption and scattering, atmospheric radiance, and atmospheric turbulence [56]. The atmospheric attenuation from molecules, particles, or liquid droplets including gases, aerosols (dust), fog, or precipitation is frequency dependent [57]. Compared with the free-space optical link, the THz link is more stable against scattering under harsh environments such as fog [58] and dust [59] conditions. The limit of mm-waves [60] and THz links [61], [62] in long distances is mainly caused by the absorption of different gases in the air, such as gaseous water vapor (H_2O) and carbon dioxide (CO_2) [57], [63]. So it is important to find the window with low atmospheric absorption through this band. High-level security is also an important aspect of realizing mm-waves and THz communications which is quite challenging to maintain with classical cryptography schemes. Quantum key distribution (QKD) can help to achieve the goal of high-level unconditional security with the power of quantum physics [64], [65], [66], [67]. QKD could be divided into discrete variables (DVQKD based on single photon sources and detectors) and continuous variables (CVQKD based on standard communication systems) [65], [66], [67], [68], [69], [70], [71], [72], [73], [74], [75], [76], [77], [78]. CVQKD uses coherent homodyne detection instead of single photon detection [68] and could be integrated with next-generation communication systems [69].

Single-input single-output (SISO) is a kind of classical communication system where the transmitter and receiver do not have several antennas. To meet the explosion of data transmission, multiple-input multiple-output (MIMO) technology has been widely used in wireless communication nowadays. A MIMO system with multiple antennas at both the transmitter and receiver side brings benefits on data throughout and communication range with limited bandwidth and transmit power [70]. THz QKD with SISO and MIMO systems was introduced in [64] and [71], with the main focus on mid- and far-infrared frequency ranges (10–40 THz) at room temperature ($T = 296$ K).

Motivated by the works of [64] and [71], this work focuses on SISO and MIMO QKD at the temperature of $T< 50$ K. We investigate CVQKD at frequency ranges of mm-waves and THz, from $f = 100$ GHz to 1 THz, with antennas and detectors both operating in the cryogenic environment ($T < 50$ K). Moreover, we compare the performance of both the SISO and MIMO CVQKD systems at this frequency range.

II. SYSTEM MODEL

For the proposed mm-waves and THz quantum communication scheme, the cryogenic antennas generate EM fields that oscillate at an angular frequency ω. This EM field is quantized and the system gets a Hamiltonian $H = h\omega(\hat{a}^\dagger\hat{a} + \frac{1}{2})$. The H is similar to the Hamiltonian of a quantum harmonic oscillator with h as Planck's constant, $\hat{a}$ as the annihilation operator, and $\hat{a}^\dagger$ as the creation operator. Moreover, the quadrature field operators $\hat{\mathrm{q}} = \frac{\hat{a}+\hat{a}^\dagger}{\sqrt{2}}$ and $\hat{\mathrm{p}} = \frac{\mathrm{i}(\hat{a}+\hat{a}^\dagger)}{\sqrt{2}}$ are dimensionless canonical observables of the system (similar to the position and momentum of the quantum harmonic oscillator) [72]. Finally, coherent states of the system are the eigenstates of the annihilation operator $\hat{a}$, provided by $\hat{a}|\alpha\rangle = \alpha|\alpha\rangle$. Here, $\alpha = q + \mathrm{i}p \in \mathrm{C}$ indicates the coherent state amplitude [71], taken from a 2-D Gaussian distribution. Two independent continuous variables q and p are used to create a secret key between Alice and Bob [64].

Notation: Boldface and italic capital letters such as $\boldsymbol{A}$ denote matrices. $\boldsymbol{A}^\dagger$ is the conjugate transpose of matrix $\boldsymbol{A}$ while $\boldsymbol{A}^T$ is the transpose. $\mathbf{0}_{M\times N} \in \mathbb{C}^{M\times N}$ is a zero-complex matrix and $\mathbf{1}_{M\times N} \in \mathbb{C}^{M\times N}$ is a complex matrix of ones. $\boldsymbol{I}_M$ represents a $M \times M$ identity matrix. A $M \times M$ diagonal matrix described by $diag(\boldsymbol{a})$ with $\boldsymbol{a} \in \mathbb{C}^M$ shows $\boldsymbol{a}$ on its diagonal. And $\mathcal{N}(\mu, \boldsymbol{\Sigma})$ is a real multivariate Gaussian distribution in which the vector is μ and the covariance matrix is $\boldsymbol{\Sigma}$.

A. CHANNEL MODEL

We consider a one-way communication channel to build a secret key between Alice and Bob as shown in Fig. 1(a). A MIMO mm-waves and THz communication channel between Alice and Bob include a transmitter with N_t antennas at Alice's side and a receiver with N_r antennas at Bob's side. We assume the antennas at both sides are distributed in a 1-D ULA with each antenna element's gain G_a. As the crosstalk between the antennas could be reduced by using proper structure and material, we ignore the crosstalk in this work [79]. So the antenna gains of Alice and Bob are $G_t = N_t G_a$ and $G_r = N_r G_a$ [71]. The Gaussian modulation of the thermal state is a widely used encoding protocol for several frequencies [64]. Alice begins with a vacuum state $|0\rangle$ and generates N_t coherent states $|a_i\rangle$ with amplitudes $a_i = Q_{A,i} + jP_{A,i}, \quad i = 1, 2, \ldots, N_t$ from the N_t antennas with quadratures being chosen from two independent random vectors $\boldsymbol{Q}$, $\boldsymbol{P} \sim \mathcal{N}(\mathbf{0}_{N_t\times 1}, V_s\boldsymbol{I}_{N_t})$ where V_s is the variance of the initial signal encoding [71]. Two quadratures $\hat{Q}_{A,i}$ and $\hat{P}_{A,i}$ of a quantum THz source (thermal) state are randomly sent by the ith antenna element of Alice and described by $\hat{X}_{A,i} \in \{\hat{Q}_{A,i}, \hat{P}_{A,i}\}$. So the ith mode of Alice can be considered as $\hat{X}_{A,i} = a_i + \hat{0}$, where $\hat{0}$ is the thermal mode (quadrature operator) due to the background thermal noise at mm-waves and THz and a_i denotes the classical modulated variable [64], [80]. The total variance of Alice's mode is

$$V_a = V_s + V_0 \tag{1}$$

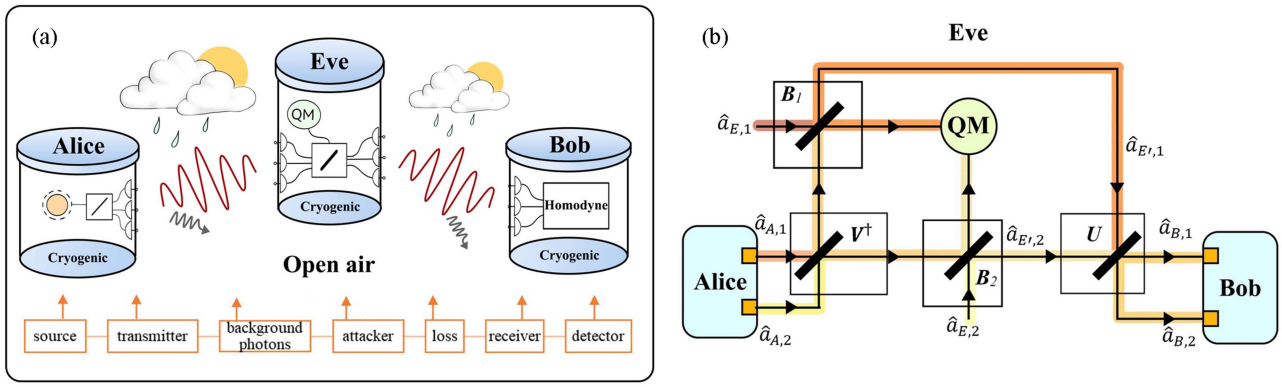

FIGURE 1. (a) System model of the proposed mm-waves and THz QKD. Alice prepares thermal states at the source which denotes a generator. The transmitter and receiver are antennas distributed in a 1-D uniform linear array (ULA). Alice, Bob, and Eve do their job at cryogenic ambient (low temperature). The channel loss through the open-air environment contains atmospheric absorption and free-space loss. Eve's output modes are stored in a quantum memory (QM). Bob uses a homodyne detector to measure quadrature. (b) Schematic of the phase shifters model described for a 2×2 MIMO system. The channel is modeled by four beam splitters. Alice generates two coherent states $\hat{a}_{A,1}$ and $\hat{a}_{A,2}$ based on random vectors and sends them out from her two antennas as thermal states. These two states are mixed by the first beam-splitter $V^\dagger$. Then Eve operates a collective Gaussian attack. She prepares two two-mode squeezed vacuum states and uses beam-splitter B_1 and B_2 to combine the input and her states. The output and one of the original modes are saved in QM. Before Bob detects the input, the signals are mixed by beam-splitter U. At last, Bob uses his two antennas to receive the modes $\hat{a}_{B,1}$ and $\hat{a}_{B,2}$.

where V_0 is the variance of thermal state (contains variance of vacuum mode and variance of preparation noise) [64]. V_0 is defined as

$$V_0 = 1 + 2\bar{n}. \tag{2}$$

Here, 1 is the vacuum shot noise unit and

$$\bar{n} = \left[\exp\left(\frac{hf_c}{k_B T}\right) - 1\right]^{-1} \tag{3}$$

is the mean thermal photon number, h is Planck's constant, k_B denotes Boltzmann's constant, T is the environment temperature, and f_c is the carrier frequency. Now, let's consider Alice sends her states to Bob (receiver) over an insecure quantum channel. Bob uses a noisy homodyne detection technique, which is based on mm-waves and THz shot-noise limited quantum detector that randomly switches between quadrature $\hat{Q}$ and $\hat{P}$, to measure the incoming thermal states.

The channel matrix between Alice and Bob could be modeled as [71], [73], [74]

$$\boldsymbol{H} = \sum_{l=1}^{L} \sqrt{\gamma_l} e^{j2\pi f_c \tau_l} \psi_{N_r}\left(\phi_{r,\mathrm{LOS}}\right) \psi_{N_t}^{\dagger}\left(\phi_{t,\mathrm{LOS}}\right) \tag{4}$$

where $\boldsymbol{H} \in \mathbb{C}^{N_r \times N_t}$, L is the full number of multipath components, τ_l is the propagation delay of the lth multipath. We only consider the line-of-sight (LOS) path with L=1 in this work. So the path loss γ_l is given by [71]

$$\gamma_{l=1} = G_t G_r \left(\frac{\lambda}{4\pi d}\right)^2 10^{-\frac{\delta d}{10}} \tag{5}$$

where d is the distance (km) between Alice and Bob and δ is the atmospheric loss and is defined as dB/km [64], [73]. It contains both the free space path and the atmospheric absorption losses of mm-waves and THz waves. $\phi_{r,\mathrm{LOS}}$ and $\phi_{t,\mathrm{LOS}}$ are the angle of arrival seen by Bob, and the angle of departure from Alice, respectively. $\psi_K(\theta)$ represents the array response vector of a ULA which contains K number of antennas.

The derivation details of the channel model are described by a singular-value decomposition (SVD) scheme introduced by Kundu et al. [71] are presented in Appendix A.

Although the coherent attack is the general attack, the works reported in [75] and [76] proved that once the system is secure against collective attacks, it is also secure against general attacks with the long secret key. In CVQKD, the most realistic and studied collective attack against Gaussian protocols is the entangling cloner attack [64]. So, we assume the channel is totally under Eve's control and she uses entangling cloners to steal information. Fig. 1(b) shows a 2 × 2 MIMO system built by four beam-splitters as an example [72]. After the two transmitted modes from Alice are combined by beam-splitter $\boldsymbol{V}^\dagger$, Eve will pick up two produced output modes. Eve should prepare two pairs of entangled Einstein–Podolsky–Rosen $\{\hat{e}_1, \hat{E}_1\}$ and $\{\hat{e}_2, \hat{E}_2\}$ (known also as two-mode squeezed vacuum states) in advance. Once received the input, Eve uses $\boldsymbol{B}_1$ and $\boldsymbol{B}_2$ to combine them with $\hat{E}_1$ and $\hat{E}_2$. The relationship between input and output of $\boldsymbol{B}_i$ can be written as [71], [72]

$$\begin{bmatrix} \hat{a}_{\mathrm{out},1} \\ \hat{a}_{\mathrm{out},2} \end{bmatrix} = \begin{bmatrix} \sqrt{\eta_i} & \sqrt{1-\eta_i} \\ -\sqrt{1-\eta_i} & \sqrt{\eta_i} \end{bmatrix} \begin{bmatrix} \hat{a}_{\mathrm{in},1} \\ \hat{a}_{\mathrm{in},2} \end{bmatrix}. \tag{6}$$

Here, η_i is the round-trip transmissivity of two port beam-splitter $\boldsymbol{B}_i$. Then Eve will save one of the outputs from every beam-splitters $(\hat{E}'_1, \hat{E}'_2)$ and the original modes $(\hat{e}_1, \hat{e}_2)$ in her QM and measure the ancilla modes to exploit information when Alice and Bob completed their classical communication. The other two output modes will be combined by the

beam-splitter $\boldsymbol{U}$ and sent to Bob. We assume Alice applies $\boldsymbol{V}$ as the base of beamforming at her end, and Bob employs $\boldsymbol{U}^{\dagger}$ as the base of decoding at his side. The whole model could be described by [71], [72]

$$\hat{\boldsymbol{a}}_B = \boldsymbol{U}^{\dagger}\boldsymbol{H}\boldsymbol{V}\hat{\boldsymbol{a}}_A + \boldsymbol{U}^{\dagger}\boldsymbol{U}\boldsymbol{S}\hat{\boldsymbol{a}}_E \tag{7}$$

where $\hat{\boldsymbol{a}}_B = [\hat{a}_{B,1}, \ldots, \hat{a}_{B,N_r}]^T$ is the received mode of Bob, $\hat{\boldsymbol{a}}_A = [\hat{a}_{A,1}, \ldots, \hat{a}_{A,N_t}]^T$ is the transmitted mode of Alice, $\hat{\boldsymbol{a}}_E = [\hat{a}_{E,1}, \ldots, \hat{a}_{E,N_t}]^T$ is the injected Gaussian mode of Eve

$$\boldsymbol{S} = \text{diag}\left\{\sqrt{1-\eta_1}, \ldots, \sqrt{1-\eta_r}, 1_{(M-r)\times 1}\right\} \tag{8}$$

is a diagonal matrix with $M = \min(N_t, N_r)$. The calculation details could be found in Appendix A. The efficient channel between Alice and Bob can be disintegrated into r parallel SISO channels by utilizing the SVD of $\boldsymbol{H}$(r is the rank of $\boldsymbol{H}$). In this case, the relation between channels' input and output can be written as [71]

$$\hat{\boldsymbol{a}}_{B,i} = \sqrt{T_i}\hat{\boldsymbol{a}}_{A,i} + \sqrt{1-T_i}\hat{\boldsymbol{a}}_{E,i}, \quad i = 1, 2, \ldots, r. \tag{9}$$

Here, T_i is the ith non-zero eigenvalue of $\boldsymbol{H}^{\dagger}\boldsymbol{H}$ and could also be considered as the ith transmissivity of the channel. Homodyne experiments on one of the randomly selected quadratures will be performed by Bob for every r-received mode and get the result detailed in Appendix A.

We set W to the variance of the thermal noise introduced by Eve. So, Bob will receive the ith mode with the shot-noise level $V(\hat{X}_{B,i}) = T_i V_0 + (1 - T_i)W$ [64]. $\hat{X}_{B,i}$ is Bob's received quadrature described by (22) in Appendix A. If Eve wants to completely hide in the background noise, she can use $W = V_0$. Then Bob will receive the shot-noise level $V(\hat{X}_{B,i}) = V_0$ which is the same as what Alice sent. Although the value of V_0 could be enlarged by frequencies below 1 THz, we could gain $V_0 \approx 1$ *SNU* by cooling down the system to low temperatures.

B. SECRET KEY RATE

In this mm-waves and THz CVQKD scheme, Alice and Bob replicate the previous quantum communication protocol several times to generate a string. Then they correct errors in their string by using reconciliation protocol. Direct reconciliation (DR) is the scheme in which Bob uses Alice's encoding string to prepare the key while reverse reconciliation (RR) is when Alice prepares the key based on Bob's decoding result. Alice and Bob use a reconciliation protocol to achieve privacy amplification to reduce the knowledge stolen by Eve [71]. In this work, we use an asymptotic secret key rate to study the performance of RR protocol in mm-waves and THz QKD. In RR, it is possible to achieve a positive secret key rate when the channel transmissivity is almost 0 while in DR it required a channel transmissivity larger than 0.5 [80] and is impractical in mm-waves and THz because of the high losses (both atmospheric absorption and path).

According to [71], the secret key rate of the MIMO system could be divided into r SISO channels. So we first analyze the secret key rate of a SISO channel. In the RR scheme, Alice and Bob use the decoding outcomes from Bob's side to generate their secret key [77]. Alice and Bob could estimate the mutual information they shared, described as $I(a:b)$, and the accessible information of Eve, described as $I(E:b)$. The asymptotic secret key rate $R^{\blacktriangleleft}$ could be described by the surplus information shared by Alice and Bob and is given by [65]

$$R^{\blacktriangleleft} = I(a:b) - I(E:b). \tag{10}$$

The mutual information between Alice and Bob is

$$I(a:b) = \frac{1}{2}\log_2\left[1 + \frac{TV_s}{\Lambda(V_0,\ W)}\right] \tag{11}$$

$$\Lambda(x, y) = Tx + (1 - \mathrm{T})\, y \tag{12}$$

while $V_s \gg V_0, W$, and Eve's information is bounded by the Holevo information $\mathrm{I}(E:b)$ which is defined as

$$I(E:b) = H_E - H_{E|b} \tag{13}$$

where H_E and $H_{E|b}$ are the von Neumann entropy of Eve's total and conditional state given by (25) and (26) in Appendix A respectively [71], [78].

The total secret key rate is finally given by the sum of r SISO links' secret key rate [71] assuming $T_i \to 0$

$$R^{\blacktriangleleft}_{\text{MIMO}} = \sum_{i=1}^{r} R_i^{\blacktriangleleft} \approx \zeta tr\left(\boldsymbol{H}^{\dagger}\boldsymbol{H}\right) - rh(W) \tag{14}$$

where

$$\zeta = 0.72\left[\frac{V_s}{W} - \ln\left(\frac{V_a+1}{V_a-1}\right)\left(\frac{V_a^2 - W^2}{2W} - V_a\right)\right] \tag{15}$$

and $tr(\boldsymbol{H}^{\dagger}\boldsymbol{H}) = \sum_{i=1}^{r} T_i$. $h(W)$ is a function given by

$$h(\mathrm{x}) = \frac{x+1}{2}\log_2\left(\frac{x+1}{2}\right) - \frac{x-1}{2}\log_2\left(\frac{x-1}{2}\right). \tag{16}$$

C. SYSTEM CONDITIONS

To achieve a positive secret key rate, $\zeta tr(\boldsymbol{H}^{\dagger}\boldsymbol{H}) > rh(W)$ is required. Verified from (1)–(4), only $\zeta tr(\boldsymbol{H}^{\dagger}\boldsymbol{H})$ in (14) depends on frequency and ζ also depends on temperature. With a given frequency, lower temperature could decrease V_0 and increase ζ in (15). This also happens with a given temperature and increasing frequency. But higher frequency normally brings higher path loss which may decrease $tr(\boldsymbol{H}^{\dagger}\boldsymbol{H})$. Since $tr(\boldsymbol{H}^{\dagger}\boldsymbol{H})>0$, the limit of $\zeta > \alpha = \frac{rh(W)}{tr(\boldsymbol{H}^{\dagger}\boldsymbol{H})}$ is equal to $\zeta > \alpha = 0$ while W=1. This condition helps us find the balance between ζ and $tr(\boldsymbol{H}^{\dagger}\boldsymbol{H})$ and get a positive secret key rate.

Fig. 2 shows ζ as a function of temperature for different frequencies in a MIMO THz QKD system [71]. According to the simulation results, we achieved secure transmission for frequencies between f= 100 GHz and 1 THz, at temperatures T< 43 K. The detail of the maximum operating temperature for each frequency is shown in Table I.

IEEE Transactions on Quantum Engineering

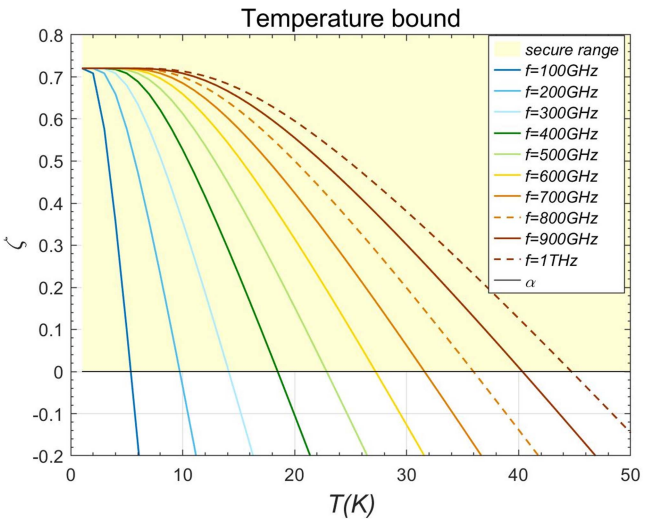

FIGURE 2. Curves show ζ as a function of temperature for different frequencies. To achieve secure transmission, ζ should keep above line α (locate in the secure range).

TABLE I Parameters and simulation results for different frequencies

Frequency	Atmospheric absorption δ	Maximum temperature T_{max} (K)	Distance of 32×32 MIMO system at T_{max} (m)
100GHz	0.4dB/km	4	700
200GHz	3dB/km	8	320
300GHz	4dB/km	13	75
400GHz	20dB/km	17	86
500GHz	50dB/km	21	68
600GHz	150dB/km	26	26
700GHz	70dB/km	30	38
800GHz	100dB/km	35	36
900GHz	100dB/km	39	25
1THz	100dB/km	43	21

III. SIMULATION RESULT

We use the secret key rate (R) to define whether the system is safe or not. A positive secret key rate reflects a safe transmission. As R of the MIMO system is the sum of the SISO systems, we also compared the different performances of the MIMO and SISO systems at the same conditions.

A. SIMULATION OF THE MIMO SYSTEM

According to [63], [57], and [81], the atmospheric absorption for each frequency is shown in Table I. We assume the target of the secret key rate is 10^{-5} bit/use [71]. Table I also shows the distance of 32 × 32 MIMO system at maximum temperature for each frequency. While $f = 700$ GHz and $f = 800$ GHz could reach more than 35 m at $T > 30$ K, $f = 600$ GHz could only get to 26 m at a lower temperature because of higher absorption at this frequency. Fig. 3(a) and (b) shows the secret key rate as a function of secure transmission distance for frequencies from $f = 100$ GHz to 1 THz at $T = 4$ K in a 32 × 32 MIMO system. The distance of $f = 100$ GHz and $f = 200$ GHz could achieve $d = 700$ m at $T = 4$ K which is the maximum through all frequencies. The secure distance for $f = 300$ GHz could get to $d = 500$ m, but it will drop to under $d = 160$ m for frequencies above $f = 500$ GHz. If the number of antennas reduces to 8 × 8, the maximum distance could still reach $d = 200$ m for $f = 200$ GHz as shown in Fig. 3(c). But for frequencies above $f = 600$ GHz in Fig. 3(d), the distances are all below 50 m because of the high absorption.

High MIMO configuration could enhance the maximum secure distance as shown in Fig. 4. While the maximum distance is $d = 700$ m for a 32 × 32 MIMO system, the secure transmission could achieve much more than $d = 8000$ m for a 1024 × 1024 MIMO at $f = 100$ GHz at $T = 4$ K as shown in Fig. 4(a). The same trend could be found for $f = 200$ GHz at $T = 8$ K and $f = 1$ THz at $T = 43$ K. For $f = 200$ GHz, the maximum distance is more than $d = 3000$ m for 1024 × 1024 MIMO at $T = 8$ K. But secure distances for $f = 1$ THz at $T = 43$ K are not as much longer because of the high channel loss caused by atmospheric absorption and thermal noise. It could only get to 160 m with a 1024 × 1024 MIMO antenna system at $T = 43$ K. And compared with Fig. 3(b), the distance for $f = 1$ THz at $T = 43$ K is just one-fifth of $T = 4$ K, with 32 × 32 antennas.

B. SIMULATION OF THE SISO SYSTEM

Compared with a large MIMO scheme, the maximum distance of a SISO scheme is shorter at frequency ranges between $f = 100$ GHz and $f = 1$ THz. We assume the target secret key rate is 10^{-5} bit/use [71]. Fig. 5(a) shows that the maximum distance in the SISO system is less than 12 m for $f = 200$ GHz at $T = 8$ K, which is much less than what is observed in a MIMO system shown in Fig. 4(b). Fig. 5(b) shows the distance for $f = 100$ GHz–1 THz in a SISO scheme at $T = 4$ K. We could find that the maximum distances decrease with higher frequency at 200 GHz–1 THz range caused by the path loss. Comparing Fig. 5(a) and (b), it is obverse that lower temperature increases the maximum distance for the same frequency.

Comparing Fig. 5(b) with Fig. 3, we find that at the same temperature, the MIMO scheme could achieve a longer distance than the SISO scheme. So it is necessary to use multiple antennas in mm-waves and THz QKD system. As frequencies $f = 800$ GHz, $f = 900$ GHz, and $f = 1$ THz have the same atmospheric absorption, Fig. 5(b) shows that the transmission distance improved by the lower frequency. This may cause by the increase of $tr(\boldsymbol{H}^{\dagger}\boldsymbol{H})$ as lower frequencies have less free-space path loss and matter more than the increase of V_0 (which in turn decreases ζ) at this range. As a result, to enhance the secure distance, we could use more antennas, cool down the temperature, or choose lower frequencies.

IV. DISCUSSION

We study through simulations of MIMO CVQKD protocol on mm-waves to THz open-air link with ideal LOS path and crosstalk-free antennas. The influences of cryogenic operating temperature for mm-waves and THz circuits and the

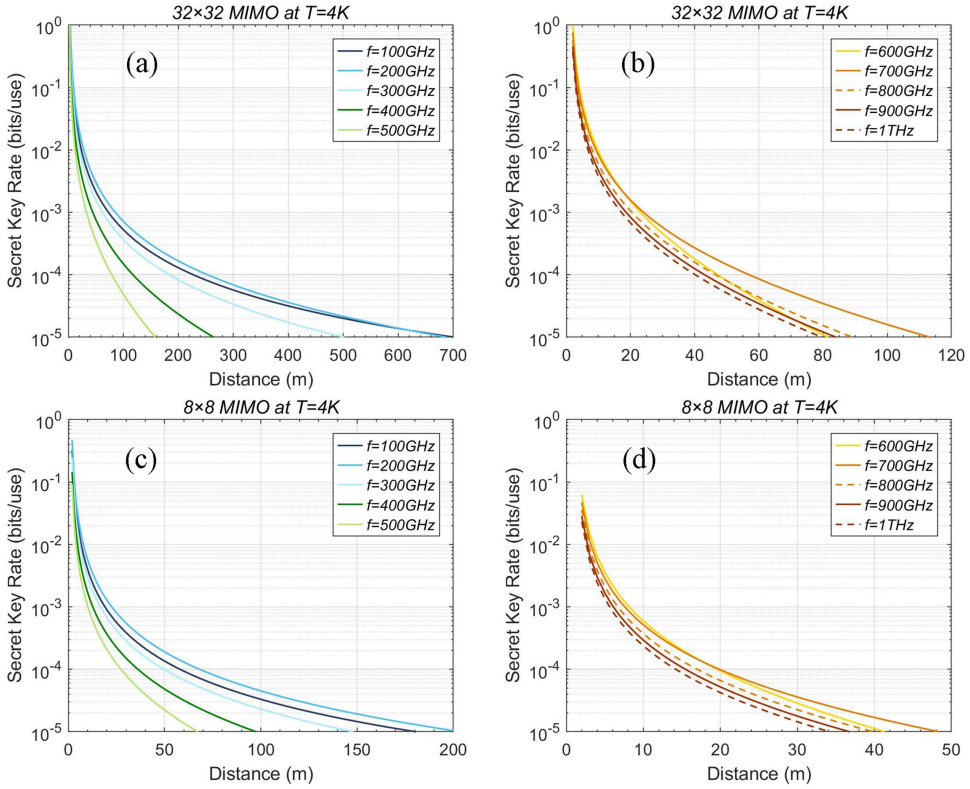

FIGURE 3. (a) Transmission distance of a 32×32 MIMO system for $f = 100$ to 500 GHz at $T = 4$ K. (b) Transmission distance of a 32×32 MIMO system for $f = 600$ to 1 THz at $T = 4$ K. (c) Transmission distance of an 8×8 MIMO system for $f = 100$ to 500 GHz under $T = 4$ K. (d) Transmission distance of an 8×8 MIMO system for $f = 600$ GHz to 1 THz under $T = 4$ K. Here, parameters are G_a=30, W=1, V_a=1000.

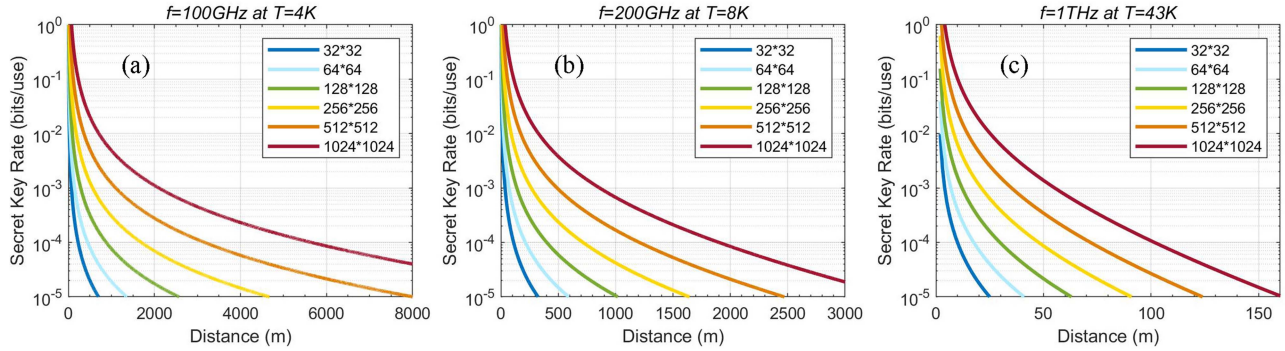

FIGURE 4. Curves show the secret key rate as a function of transmission distance for the different numbers of antennas in MIMO systems. (a) Result for $f = 100$ GHz, at $T = 4$ K. (b) Result for $f = 200$ GHz, at $T = 8$ K. (c) Result for $f = 1$ THz, at $T = 43$ K.

number of antennas are considered by assuming the perfect quality of the beam-splitter and communication channel. Although the MIMO array may overcome high path loss by using proper beamforming protocol and reduce the interference by using highly directional antennas [82], for the realization of the mm-waves and THz CVQKD in the future, except the channel loss caused by atmospheric absorption, the co-channel interference, intercell interference, non-LOS path, and multipath effect all should be considered in the channel loss [83], [84].

Recently, devices for mm-waves to THz frequency range based on superconductors operating at temperature ranges from 4 to 80 K [3] such as efficient coherent emitters [18], THz photonic circuits [46], etc. have been proposed, which could be the possible solution of building the cryogenic mm-wave to THz quantum communication link. The super conducting-based coherent THz source has been reported to generate high-power THz radiation ($>\mu$W) below 50 K [85] that abandons the complicated THz -optics conversion and is suitable for on-chip mm-waves and THz waves transmission.

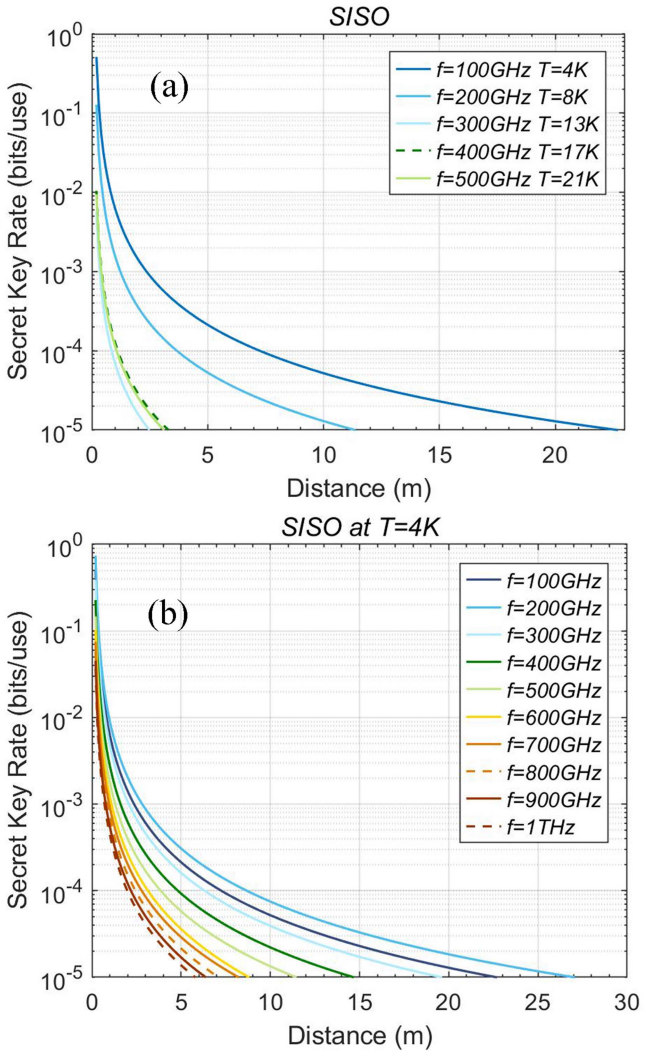

FIGURE 5. (a) Secret key rate R as a function of transmission distance for SISO for frequency ranges between $f = 100$ GHz and $f = 500$ GHz at the highest operational temperature. Atmospheric absorptions in the channel are shown in Table I. (b) Secret key rate R as a function of transmission distance for SISO for frequency ranges between $f = 100$ GHz and $f = 1$ THz at $T = 4$ K.

A recent THz hybrid superconductor circuit cavity has been proposed that may help the realization of coherent THz detectors at 20 K [86].

Even so, many research efforts are still needed to accomplish the whole scheme in practical hardware. For example, a highly directional antenna or source for THz on-chip circuits is an important foundation against interference and achieving long-distance communication. THz detector without optical THz conversion may increase the flexibility and efficiency of the communication. As the optical CVQKD has been realized and proved to be achievable with megabits per second rate over kilometers [87], [88], we believe the mm-waves to THz CVQKD system is not so far from accomplishment.

IV. CONCLUSION

In this work, for the first time, we developed SISO and MIMO QKD schemes in mm-waves and THz frequency ranges, from $f = 0.1$ to $f = 1$ THz, with the cryogenic operation of sources and detectors below $T = 50$ K. We found that a positive secret key rate can be observed at the targeted frequency range. MIMO technology could improve the secure transmission distance compared with the SISO scheme. Moreover, we showed that the more antennas are in the system the longer transmission distance could be achieved. To build a long-way secure communication channel, more antennas, low-temperature operation, and lower frequencies are required. We also discussed the practical hardware realization possibility of the cryogenic mm-waves and THz system and have given our views of the development direction in both experimental and theoretical aspects for the mm-waves and THz QKD. Our work may guide the effort in the development of next-generation secure wireless communication systems and the establishment of quantum internet for applications from satellites to indoor and short-distance communications.

APPENDIX A

A. COMPUTATION OF CHANNEL MODEL

The channel matrix between Alice and Bob could be modeled as (4)

$$\boldsymbol{H} = \sum_{l=1}^{L} \sqrt{\gamma_l} e^{j2\pi f_c \tau_l} \psi_{N_r}\left(\phi_{r,LOS}\right) \psi_{N_t}^{\dagger}\left(\phi_{t,LOS}\right)$$

where $\boldsymbol{H} \in \mathbb{C}^{N_r \times N_t}$, L is the full number of multipath components, τ_l is the propagation delay of the lth multipath. The path loss γ_l for the LOS path (L=1) is given by (5)

$$\gamma_{l=1} = G_t G_r \left(\frac{\lambda}{4\pi d}\right)^2 10^{-\frac{\delta d}{10}}$$

where d is the distance (km) between Alice and Bob and δ is the atmospheric loss. $\phi_{r,\mathrm{LOS}}$ and $\phi_{t,\mathrm{LOS}}$ is the angle of arrival seen by Bob, and the angle of departure from Alice, respectively. $\psi_K(\theta)$ represents the array response vector of a ULA which contains K number of antennas [71]

$$\psi_K(\theta) = \frac{1}{\sqrt{K}}\left[1,\ e^{j2\pi \frac{d_a}{\lambda}\sin\theta},\ \ldots,\ e^{j2\pi \frac{d_a}{\lambda}(K-1)\sin\theta}\right]^T \quad (17)$$

Here, d_a and λ denote the inter-antenna spacing and wavelength of the carrier signal, respectively. We assume $d_a = \lambda/4$ in this work. The channel model could be described by a SVD scheme introduced by [71]

$$\boldsymbol{H} = \boldsymbol{U}\boldsymbol{\Sigma}\boldsymbol{V}^{\dagger} \quad (18)$$

Here, $\boldsymbol{U} \in \mathbb{C}^{N_r \times N_r}$ and $\boldsymbol{V} \in \mathbb{C}^{N_t \times N_t}$ are unitary matrices represent K phase shifters [72], and $\boldsymbol{\Sigma}$ is given as

$$\boldsymbol{\Sigma} = \begin{bmatrix} \mathrm{diag}\left\{\sqrt{\eta_1}, \ldots, \sqrt{\eta_r}\right\} & \mathbf{0}_{r\times(N_t-r)} \\ \mathbf{0}_{(N_r-r)\times r} & \mathbf{0}_{(N_r-r)\times(N_t-r)} \end{bmatrix} \quad (19)$$

where r is the rank of $\boldsymbol{H}$ and $\sqrt{\eta_1}, \ldots, \sqrt{\eta_r}$ are the r nonzero singular values of $\boldsymbol{H}$ generated by the transmissivity of beam-splitters in the system [72].

As shown in Fig. 1(b), the whole model of a MIMO system could be described by [71], [72]

$$\hat{\boldsymbol{a}}_B = \boldsymbol{U}^{\dagger}\boldsymbol{H}\boldsymbol{V}\hat{\boldsymbol{a}}_A + \boldsymbol{U}^{\dagger}\boldsymbol{U}\boldsymbol{S}\hat{\boldsymbol{a}}_E \tag{20}$$

where $\hat{\boldsymbol{a}}_B = [\hat{a}_{B,1}, \ldots, \hat{a}_{B,N_r}]^T$ is the received mode of Bob, $\hat{\boldsymbol{a}}_A = [\hat{a}_{A,1}, \ldots, \hat{a}_{A,N_t}]^T$ is the transmitted mode of Alice, $\hat{\boldsymbol{a}}_E = [\hat{a}_{E,1}, \ldots, \hat{a}_{E,N_t}]^T$ is the injected Gaussian mode of Eve.

$$\boldsymbol{S} = \text{diag}\left\{\sqrt{1-\eta_1}, \ldots, \sqrt{1-\eta_r}, 1_{(M-r)\times 1}\right\} \tag{21}$$

is a diagonal matrix with $M = \min(N_t, N_r)$. We get $\boldsymbol{U}^{\dagger}\boldsymbol{U} = \boldsymbol{I}_{N_r}$ and $\boldsymbol{V}^{\dagger}\boldsymbol{V} = \boldsymbol{I}_{N_t}$ as $\boldsymbol{U}$ and $\boldsymbol{V}$ are unitary matrices. Considering (18) $\boldsymbol{H} = \boldsymbol{U}\boldsymbol{\Sigma}\boldsymbol{V}^{\dagger}$, diagonal matrix $\boldsymbol{\Sigma}$ and $\boldsymbol{S}$, (20) would turn to $\hat{\boldsymbol{a}}_B = \boldsymbol{U}^{\dagger}\boldsymbol{U}\boldsymbol{\Sigma}\boldsymbol{V}^{\dagger}\boldsymbol{V}\hat{\boldsymbol{a}}_A + \boldsymbol{U}^{\dagger}\boldsymbol{U}\boldsymbol{S}\hat{\boldsymbol{a}}_E = \boldsymbol{\Sigma}\hat{\boldsymbol{a}}_A + \boldsymbol{S}\hat{\boldsymbol{a}}_E$. So the efficient channel between Alice and Bob can be disintegrated into r parallel SISO channels.

Bob randomly chooses quadratures for his input and operates homodyne measurements. Then the input-output relationship of ith parallel channel between Bob's received quadrature $\hat{X}_{B,i}$ and Alice's transmitted quadrature $\hat{X}_{A,i}$ can be written by a generic quantum channel as [71]

$$\hat{X}_{B,i} = \sqrt{T_i}\hat{X}_{A,i} + \sqrt{1-T_i}\hat{X}_{E,i}, \quad i = 1, 2, \ldots, r \tag{22}$$

with T_i and $\hat{X}_{E,i}$ as transmittance, and Eve's excess noise quadrature, respectively. We can write for Eve's ancilla mode

$$\hat{X}_{E',i} = -\sqrt{1-T_i}\hat{X}_{A,i} + \sqrt{T_i}\hat{X}_{E,i}, \quad i = 1, 2, \ldots, r. \tag{23}$$

B. COMPUTATION OF THE SECRET KEY RATE

The secret key rate $R^{\blacktriangleleft} = I(a:b) - I(E:b)$ is given by mutual information. Assuming Gaussian statistic for simulating purposes, the mutual information between Alice and Bob is

$$I(a:b) = \frac{1}{2}\log_2\left[1 + \frac{TV_s}{\Lambda(V_0,\ W)}\right]$$

$$\Lambda(x, y) = Tx + (1 - \mathrm{T})\, y.$$

And Eve's information is bounded by the Holevo information $I(E:b)$ which is defined as

$$I(E:b) = H_E - H_{E|b} \tag{24}$$

$$H_E = h(v_1) + h(v_2) \tag{25}$$

$$H_{E|b} = h(v_3) + h(v_4) \tag{26}$$

where H_E and $H_{E|b}$ are the von Neumann entropy of Eve's total and conditional state, respectively, [71], [78]. The von Neumann entropy depends on symplectic eigenvalues as given by [71]

$$v_1 = \Lambda(W, V_a),\ v_2 = \mathrm{W} \tag{27}$$

$$v_3,\ v_4 = \sqrt{\frac{1}{2}\left(\Delta \pm \sqrt{\Delta^2 - 4\Upsilon}\right)} \tag{28}$$

and

$$\Delta = \frac{V_a W \Lambda(W,\ V_a) + W\Lambda(WV_a,\ 1)}{\Lambda(V_a,\ W)} \tag{29}$$

$$\Upsilon = \frac{V_a W^2 \Lambda(W,\ V_a)\,\Lambda(WV_a,\ 1)}{\Lambda^2(V_a,\ W)}. \tag{30}$$

The function $h(x)$ is defined as

$$h(\mathrm{x}) = \frac{x+1}{2}\log_2\left(\frac{x+1}{2}\right) - \frac{x-1}{2}\log_2\left(\frac{x-1}{2}\right). \tag{31}$$

REFERENCES

[1] T. Nagatsuma et al., "Terahertz wireless communications based on photonics technologies," *Opt. Exp.*, vol. 21, no. 20, pp. 23736–23747, 2013, doi: 10.1364/OE.21.023736.

[2] D. M. M. T. Kürner and T. Nagatsuma, *THz Communications: Paving the Way Towards Wireless Tbps*. Berlin, Germany: Springer, doi: 10.1007/978-3-030-73738-2.

[3] K. Delfanazari, R. A. Klemm, H. J. Joyce, D. A. Ritchie, and K. Kadowaki, "Integrated, portable, tunable, and coherent terahertz sources and sensitive detectors based on layered superconductors," *Proc. IEEE*, vol. 108, no. 5, pp. 721–734, May 2020, doi: 10.1109/JPROC.2019.2958810.

[4] H. Elayan, O. Amin, R. M. Shubair, and M. S. Alouini, "Terahertz communication: The opportunities of wireless technology beyond 5G," in *Proc. Int. Conf. Adv. Commun. Technol. Netw.*, 2018, pp. 1–5, doi: 10.1109/COMMNET.2018.8360286.

[5] K. Kadowaki et al., "Quantum terahertz electronics (QTE) using coherent radiation from high temperature superconducting $Bi_2Sr_2CaCu_2O_{8+\delta}$ intrinsic Josephson junctions," *Physica C, Supercond.*, vol. 491, pp. 2–6, 2013, doi: 10.1016/j.physc.2013.04.011.

[6] M. J. Fitch and R. Osiander, "Terahertz waves for communications and sensing," *Johns Hopkins APL Tech. Dig.*, vol. 25, no. 4, pp. 348–355, 2004. [Online]. Available: https://www.jhuapl.edu/Content/techdigest/pdf/V25-N04/25-04-Fitch.pdf

[7] Z. T. Ma, Z. X. Geng, Z. Y. Fan, J. Liu, and H. D. Chen, "Modulators for terahertz communication: The current state of the art," *Research*, vol. 2019, 2019, Art. no. 6482975, doi: 10.34133/2019/6482975.

[8] Z. Chen et al., "A survey on terahertz communications," *China Commun.*, vol. 16, no. 2, pp. 1–35, 2019, doi: 10.12676/j.cc.2019.02.001.

[9] Z. Chen et al., "Terahertz wireless communications for 2030 and beyond: A cutting-edge frontier," *IEEE Commun. Mag.*, vol. 59, no. 11, pp. 66–72, Nov. 2021, doi: 10.1109/MCOM.011.2100195.

[10] H. Sarieddeen, M. S. Alouini, and T. Y. Al-Naffouri, "An overview of signal processing techniques for terahertz communications," *Proc. IEEE*, vol. 109, no. 10, pp. 1628–1665, Oct. 2021, doi: 10.1109/JPROC.2021.3100811.

[11] H. J. Song and T. Nagatsuma, "Present and future of terahertz communications," *IEEE Trans. Terahertz Sci. Technol.*, vol. 1, no. 1, pp. 256–263, Sep. 2011, doi: 10.1109/TTHZ.2011.2159552.

[12] M. Tsujimoto et al., "Broadly tunable subterahertz emission from internal branches of the current-voltage characteristics of superconducting $Bi_2Sr_2CaCu_2O_{8+\delta}$ single crystals," *Phys. Rev. Lett.*, vol. 108, no. 10, 2012, Art. no. 107006, doi: 10.1103/PhysRevLett.108.107006.

[13] K. Delfanazari et al., "Terahertz oscillating devices based upon the intrinsic Josephson junctions in a high temperature superconductor," *J. Infrared Millim. Terahertz Waves*, vol. 35, no. 1, pp. 131–146, 2014, doi: 10.1007/s10762-013-0027-y.

[14] I. F. Akyildiz, C. Han, Z. Hu, S. Nie, and J. M. Jornet, "Terahertz band communication: An old problem revisited and research directions for the next decade," *IEEE Trans. Commun.*, vol. 70, no. 6, pp. 4250–4285, Jun. 2022, doi: 10.1109/TCOMM.2022.3171800.

[15] K. Delfanazari et al., "Experimental and theoretical studies of mesas of several geometries for terahertz wave radiation from the intrinsic Josephson junctions in superconducting $Bi_2Sr_2CaCu_2O_{8+\delta}$," in *Proc. 37th Int. Conf. Infrared, Millim., Terahertz Waves*, 2012, pp. 1–2, doi: 10.1109/IRMMW-THz.2012.6380230.

[16] R. H. Caverly, "Breakthroughs in microwaves: Programmable terahertz chip-scale surfaces and systems—An interview with Dr. Kaushik Sengupta," *IEEE J. Microw.*, vol. 1, no. 4, pp. 853–863, Oct. 2021, doi: 10.1109/JMW.2021.3107423.

[17] K. Delfanazari et al., "Tunable terahertz emission from the intrinsic Josephson junctions in acute isosceles triangular $Bi_2Sr_2CaCu_2O_{8+\delta}$ mesas," *Opt. Exp.*, vol. 21, no. 2, pp. 2171–2184, 2013, doi: 10.1364/OE.21.002171.

[18] T. Kashiwagi et al., "High temperature superconductor terahertz emitters: Fundamental physics and its applications," *Jpn. J. Appl. Phys.*, vol. 51, no. 1, 2012, Art. no. 010113, doi: 10.1143/JJAP.51.010113.

[19] T. Kashiwagi et al., "Efficient fabrication of intrinsic-Josephson-junction terahertz oscillators with greatly reduced self-heating effects," *Phys. Rev. Appl.*, vol. 4, no. 5, 2015, Art. no. 054018, doi: 10.1103/PhysRevApplied.4.054018.

[20] T. Kashiwagi et al., "Study of radiation characteristics of intrinsic Josephson junction terahertz emitters with different thickness of $Bi_2Sr_2CaCu_2O_{8+\delta}$ crystals," *Materials*, vol. 14, no. 5, 2021, Art. no. 1135, doi: 10.3390/ma14051135.

[21] K. Delfanazari et al., "Effect of bias electrode position on terahertz radiation from pentagonal mesas of superconducting $Bi_2Sr_2CaCu_2O_{8+\delta}$," *IEEE Trans. Terahertz Sci. Technol.*, vol. 5, no. 3, pp. 505–511, May 2015, doi: 10.1109/TTHZ.2015.2409552.

[22] Y. Xiong, T. Kashiwagi, R. A. Klemm, K. Kadowaki, and K. Delfanazari, "Engineering the cavity modes and polarization in integrated superconducting coherent terahertz emitters," in *Proc. 45th Int. Conf. Infrared, Millim., Terahertz Waves*, 2020, pp. 1–2, doi: 10.1109/IRMMW-THz46771.2020.9370587.

[23] K. Delfanazari et al., "Study of coherent and continuous terahertz wave emission in equilateral triangular mesas of superconducting $Bi_2Sr_2CaCu_2O_{8+\delta}$ intrinsic Josephson junctions," *Physica C-Supercond. Appl.*, vol. 491, pp. 16–19, 2013, doi: 10.1016/j.physc.2012.12.009.

[24] Y. Saiwai et al., "Liquid helium-free high-Tc superconducting terahertz emission system and its applications," *Jpn. J. Appl. Phys.*, vol. 59, no. 10, 2020, Art. no. 105004, doi: 10.35848/1347-4065/abb8f1.

[25] K. A. Fedorova et al., "Widely tunable terahertz-generating semiconductor disk laser," *Physica Status Solidi (RRL) – Rapid Res. Lett.*, vol. 14, no. 10, 2020, Art. no. 2000204, doi: 10.1002/pssr.202000204.

[26] R. Cattaneo, E. A. Borodianskyi, A. A. Kalenyuk, and V. M. Krasnov, "Superconducting terahertz sources with 12% power efficiency," *Phys. Rev. Appl.*, vol. 16, no. 6, 2021, Art. no. L061001, doi: 10.1103/PhysRevApplied.16.L061001.

[27] J. R. Rain et al., "Wave functions for high-symmetry, thin microstrip antennas, and two-dimensional quantum boxes," *Phys. Rev. A*, vol. 104, no. 6, 2021, Art. no. 062205, doi: 10.1103/PhysRevA.104.062205.

[28] Y. Xiong and K. Delfanazari, "Engineering circular polarization in chip-integrated high-Tc superconducting THz antennas," in *Proc. Photon. Electromagn. Res. Symp.*, 2021, pp. 1016–1019, doi: 10.1109/PIERS53385.2021.9694960.

[29] Y. Xie, N. Bai, W. Hong, and X. Sun, "Study of a hexagonal lattice defect photonic crystal waveguide slow wave structure for G-band traveling wave tube," *J. Electromagn. Waves Appl.*, vol. 36, no. 6, pp. 843–855, 2022, doi: 10.1080/09205071.2021.1988870.

[30] D. P. Cerkoney et al., "Cavity mode enhancement of terahertz emission from equilateral triangular microstrip antennas of the high-Tc superconductor $Bi_2Sr_2CaCu_2O_{8+\delta}$," *J. Phys., Condens. Matter*, vol. 29, no. 1, 2017, Art. no. 015601, doi: 10.1088/0953-8984/29/1/015601.

[31] R. A. Klemm et al., "Modeling the electromagnetic cavity mode contributions to the THz emission from triangular $Bi_2Sr_2CaCu_2O_{8+\delta}$ mesas," *Physica C, Supercond.*, vol. 491, pp. 30–34, 2013, doi: 10.1016/j.physc.2012.11.006.

[32] S. Kalhor, M. Ghanaatshoar, and K. Delfanazari, "On-chip superconducting THz metamaterial bandpass filter," in *Proc. 45th Int. Conf. Infrared, Millim., Terahertz Waves*, 2020, pp. 1–2, doi: 10.1109/IRMMW-THz46771.2020.9370663.

[33] K. Yang, S. Liu, S. Arezoomandan, A. Nahata, and B. Sensale-Rodriguez, "Graphene-based tunable metamaterial terahertz filters," *Appl. Phys. Lett.*, vol. 105, no. 9, 2014, Art. no. 093105, doi: 10.1063/1.4894807.

[34] I. J. H. McCrindle, J. Grant, T. D. Drysdale, and D. R. S. Cumming, "Multi-spectral materials: Hybridisation of optical plasmonic filters and a terahertz metamaterial absorber," *Adv. Opt. Mater.*, vol. 2, no. 2, pp. 149–153, 2014, doi: 10.1364/OE.24.003451.

[35] S. Kalhor, M. Ghanaatshoar, H. J. Joyce, D. A. Ritchie, K. Kadowaki, and K. Delfanazari, "Millimeter-wave-to-terahertz superconducting plasmonic waveguides for integrated nanophotonics at cryogenic temperatures," *Materials*, vol. 14, no. 15, 2021, Art. no. 4291, doi: 10.3390/ma14154291.

[36] S. Atakaramians, S. Afshar V, T. M. Monro, and D. Abbott, "Terahertz dielectric waveguides," *Adv. Opt. Photon.*, vol. 5, no. 2, pp. 169–215, 2013, doi: 10.1364/AOP.5.000169.

[37] S. Kalhor, M. Ghanaatshoar, and K. Delfanazari, "Guiding of terahertz photons in superconducting nano-circuits," in *Proc. Int. Conf. U.K.-China Emerg. Technol.*, 2020, pp. 1–3, doi: 10.1109/UCET51115.2020.9205480.

[38] G. Gallot, S. P. Jamison, R. W. McGowan, and D. Grischkowsky, "Terahertz waveguides," *J. Opt. Soc. Amer. B*, vol. 17, no. 5, pp. 851–863, 2000, doi: 10.1364/JOSAB.17.000851.

[39] K. Wang and D. M. Mittleman, "Metal wires for terahertz wave guiding," *Nature*, vol. 432, no. 7015, pp. 376–379, 2004, doi: 10.1038/nature03040.

[40] S. Kalhor, M. Ghanaatshoar, T. Kashiwagi, K. Kadowaki, M. J. Kelly, and K. Delfanazari, "Thermal tuning of high-T-c superconducting $Bi_2Sr_2CaCu_2O_{8+\delta}$ terahertz metamaterial," *IEEE Photon. J.*, vol. 9, no. 5, Oct. 2017, Art no. 1400308, doi: 10.17863/CAM.13319.

[41] R. Degl'Innocenti, H. Lin, and M. Navarro-Cía, "Recent progress in terahertz metamaterial modulators," *Nanophotonics*, vol. 11, no. 8, pp. 1485–1514, 2022, doi: 10.1515/nanoph-2021-0803.

[42] V. Savinov, K. Delfanazari, V. A. Fedotov, and N. I. Zheludev, "Giant nonlinearity in a superconducting sub-terahertz metamaterial," *Appl. Phys. Lett.*, vol. 108, no. 10, 2016, Art. no. 101107, doi: 10.1063/1.4943649.

[43] A. S. Malishevskii and S. A. Uryupin, "On Cherenkov excitation of electromagnetic waves by vortex travelling in Josephson sandwich," *Physica Scripta*, vol. 97, no. 5, 2022, Art. no. 055817, doi: 10.1088/1402-4896/ac6546.

[44] S. Kalhor et al., "Active terahertz modulator and slow light metamaterial devices with hybrid graphene-superconductor photonic integrated circuits," *Nanomaterials*, vol. 11, no. 11, 2021, Art. no. 2999, doi: 10.3390/nano11112999.

[45] A. Squires, X. Gao, T. van der Laan, Z. Han, and J. Du, "Adding a tuneable response to a terahertz metasurface using a graphene thin film," *J. Infrared, Millim., Terahertz Waves*, vol. 43, no. 9, pp. 806–818, 2022, doi: 10.1007/s10762-022-00883-1.

[46] S. Kalhor et al., "Active terahertz modulator and slow light metamaterial devices with hybrid graphene-superconductor coupled split-ring resonator arrays," in *Proc. Photon. Electromagn. Res. Symp.*, 2022, pp. 967–971, doi: 10.1109/PIERS55526.2022.9792980.

[47] S. J. Kindness et al., "A terahertz chiral metamaterial modulator," *Adv. Opt. Mater.*, vol. 8, no. 21, 2020, Art. no. 2000581, doi: 10.1002/adom.202000581.

[48] C. Li et al., "Electrically terahertz switchable device based on superconducting composite structure metamaterial," *Appl. Phys. Lett.*, vol. 121, no. 3, 2022, Art. no. 031702, doi: 10.1063/5.0100561.

[49] S. J. Kindness et al., "Graphene-integrated metamaterial device for all-electrical polarization control of terahertz quantum cascade lasers," *ACS Photon.*, vol. 6, no. 6, pp. 1547–1555, 2019, doi: 10.1021/acsphotonics.9b00411.

[50] F. Sizov and A. Rogalski, "THz detectors," *Prog. Quantum Electron.*, vol. 34, no. 5, pp. 278–347, 2010, doi: 10.1016/j.pquantelec.2010.06.002.

[51] S. Castilla et al., "Fast and sensitive terahertz detection using an antenna-integrated graphene PN junction," *Nano Lett.*, vol. 19, no. 5, pp. 2765–2773, 2019, doi: 10.1021/acs.nanolett.8b04171.

[52] R. A. Lewis, "A review of terahertz detectors," *J. Phys. D: Appl. Phys.*, vol. 52, no. 43, 2019, Art. no. 433001, doi: 10.1088/1361-6463/ab31d5.

[53] M. Zhang, P. Foshat, S. P. Khanjari, M. Imran, M. Weides, and K. Delfanazari, "Microwave quantum key distribution with cryogenic microwave components for superconducting quantum computing," in *Proc. Int. Symp. Quantum Comput., Circuits Syst. Automat. Appl.*, Jul. 2022.

[54] P. Magnard et al., "Microwave quantum link between superconduc ting circuits housed in spatially separated cryogenic systems," *Phys. Rev. Lett.*, vol. 125, no. 26, 2020, Art. no. 260502, doi: 10.1103/PhysRevLett.125.260502.

[55] F. K. F. Florian et al., "Perspectives of microwave quantum key distribution in open-air," 2022, *arXiv:2203.05530*, doi: 10.48550/arXiv.2203.05530.

[56] H. Hemmati and D. Caplan, "Optical satellite communications," in *Optical Fiber Telecommunications: Systems and Networks*, I. P. Kaminow, T. Li, and A. E. Willner, Eds. New York, NY, USA: Academic, 2013, pp. 121–162. [Online]. Available: https://www.elsevier.com/books/optical-fiber-telecommunications-volume-vib/kaminow/978-0-12-396960-6

[57] J. Sun, F. Hu, and S. Lucyszyn, "Predicting atmospheric attenuation under pristine conditions between 0.1 and 100 THz," *IEEE Access*, vol. 4, pp. 9377–9399, 2016, doi: 10.1109/ACCESS.2016.2626200.

[58] Y. Yang, M. Mandehgar, and D. R. Grischkowsky, "Broadband THz signals propagate through dense fog," *IEEE Photon. Technol. Lett.*, vol. 27, no. 4, pp. 383–386, Feb. 2015, doi: 10.1109/LPT.2014.2375795.

[59] K. Su, L. Moeller, R. B. Barat, and J. F. Federici, "Experimental comparison of terahertz and infrared data signal attenuation in dust clouds," *J. Opt. Soc. Amer. A*, vol. 29, no. 11, pp. 2360–2366, 2012, doi: 10.1364/JOSAA.29.002360.

[60] M. Karmoose, C. Fragouli, S. Diggavi, R. Misoczki, L. L. Yang, and Z. L. Zhang, "Using mm-waves for secret key establishment," *IEEE Commun. Lett.*, vol. 23, no. 6, pp. 1077–1080, Jun. 2019, doi: 10.1109/LCOMM.2019.2909918.

[61] Z. Q. Wang, R. Malaney, and J. Green, "Inter-satellite quantum key distribution at terahertz frequencies," in *Proc. IEEE Int. Conf. Commun.*, 2019, pp. 1–7, doi: 10.1109/ICC.2019.8761168.

[62] Y. Q. He, Y. Y. Mao, D. Huang, Q. Liao, and Y. Guo, "Indoor channel modeling for continuous variable quantum key distribution in the terahertz band," *Opt. Exp.*, vol. 28, no. 22, pp. 32386–32402, 2020, doi: 10.1364/OE.405020.

[63] T. Schneider, A. Wiatrek, S. Preussler, M. Grigat, and R. P. Braun, "Link budget analysis for terahertz fixed wireless links," *IEEE Trans. Terahertz Sci. Technol.*, vol. 2, no. 2, pp. 250–256, Mar. 2012, doi: 10.1109/TTHZ.2011.2182118.

[64] C. Ottaviani et al., "Terahertz quantum cryptography," *IEEE J. Sel. Areas Commun.*, vol. 38, no. 3, pp. 483–495, Mar. 2020, doi: 10.1109/JSAC.2020.2968973.

[65] S. Pirandola et al., "Advances in quantum cryptography," *Adv. Opt. Photon.*, vol. 12, no. 4, pp. 1012–1236, 2020, doi: 10.48550/arXiv.1906.01645.

[66] S. Pirandola, R. Laurenza, C. Ottaviani, and L. Banchi, "Fundamental limits of repeaterless quantum communications," *Nature Commun.*, vol. 8, 2017, Art. no. 15043, doi: 10.48550/arXiv.1510.08863.

[67] S. Pirandola, "Composable security for continuous variable quantum key distribution: Trust levels and practical key rates in wired and wireless networks," *Phys. Rev. Res.*, vol. 3, no. 4, 2021, Art. no. 043014, doi: 10.48550/arXiv.2203.00706.

[68] I. H. L. Grande, S. Etcheverry, J. Aldama, S. Ghasemi, D. Nolan, and V. Pruneri, "Adaptable transmitter for discrete and continuous variable quantum key distribution," *Opt. Exp.*, vol. 29, no. 10, pp. 14815–14827, 2021, doi: 10.1364/OE.425382.

[69] C. Liu, C. Zhu, X. Liu, M. Nie, H. Yang, and C. X. Pei, "Multicarrier multiplexing continuous-variable quantum key distribution at terahertz bands under indoor environment and in inter-satellite links communication," *IEEE Photon. J.*, vol. 13, no. 4, Aug. 2021, Art no. 7600113, doi: 10.1109/JPHOT.2021.3098717.

[70] R. H. Shi, J. J. Shi, Y. Guo, X. Q. Peng, and M. H. Lee, "Quantum MIMO communication scheme based on quantum teleportation with triplet states," *Int. J. Theor. Phys.*, vol. 50, no. 8, pp. 2334–2346, 2011, doi: 10.1007/s10773-011-0716-z.

[71] N. K. Kundu, S. P. Dash, M. R. McKay, and R. K. Mallik, "MIMO terahertz quantum key distribution," *IEEE Commun. Lett.*, vol. 25, no. 10, pp. 3345–3349, Oct. 2021, doi: 10.48550/arXiv.2105.03642.

[72] R. Jantti, R. Di Candia, R. F. Duan, and K. Ruttik, "Multiantenna quantum backscatter communications," in *Proc. IEEE 36th Glob. Commun. Conf.*, 2017, pp. 1–6, doi: 10.1109/GLOCOMW.2017.8269081.

[73] H. Deng and A. Sayeed, "Mm-Wave MIMO channel modeling and user localization using sparse beamspace signatures," in *Proc. IEEE 15th Int. Workshop Signal Process. Adv. Wireless Commun.*, 2014, pp. 130–134, doi: 10.1109/SPAWC.2014.6941331.

[74] S. A. Busari, K. M. S. Huq, S. Mumtaz, and J. Rodriguez, "Terahertz massive MIMO for beyond-5G wireless communication," in *Proc. IEEE Int. Conf. Commun.*, 2019, pp. 1–6, doi: 10.1109/ICC.2019.8761371.

[75] B. Kraus, N. Gisin, and R. Renner, "Lower and upper bounds on the secret-key rate for quantum key distribution protocols using one-way classical communication," *Phys. Rev. Lett.*, vol. 95, no. 8, 2005, Art. no. 080501, doi: 10.1103/PhysRevLett.95.080501.

[76] R. Renner and J. I. Cirac, "de Finetti representation theorem for infinite-dimensional quantum systems and applications to quantum cryptography," *Phys. Rev. Lett.*, vol. 102, no. 11, 2009, Art. no. 110504, doi: 10.1103/PhysRevLett.102.110504.

[77] F. Grosshans, G. Van Assche, J. Wenger, R. Brouri, N. J. Cerf, and P. Grangier, "Quantum key distribution using Gaussian-modulated coherent states," *Nature*, vol. 421, no. 6920, pp. 238–241, 2003, doi: 10.1038/nature01289.

[78] C. Weedbrook et al., "Gaussian quantum information," *Rev. Modern Phys.*, vol. 84, no. 2, pp. 621–669, 2012, doi: 10.1103/RevModPhys.84.621.

[79] Y. Liao, K. Wang, H. Zhu, and X. Ji, "Crosstalk in CMOS terahertz detector array with on-chip SPR antenna," *IEEE Photon. J.*, vol. 14, no. 6, Dec. 2022, Art no. 5955506, doi: 10.1109/JPHOT.2022.3168838.

[80] C. Weedbrook, S. Pirandola, S. Lloyd, and T. C. Ralph, "Quantum cryptography approaching the classical limit," *Phys. Rev. Lett.*, vol. 105, no. 11, 2010, Art. no. 110501, doi: 10.48550/arXiv.1004.3345.

[81] Y. H. Yang, A. Shutler, and D. Grischkowsky, "Measurement of the transmission of the atmosphere from 0.2 to 2 THz," *Opt. Exp.*, vol. 19, no. 9, pp. 8830–8838, 2011, doi: 10.1364/OE.19.008830.

[82] H. Guerboukha et al., "Efficient leaky-wave antennas at terahertz frequencies generating highly directional beams," *Appl. Phys. Lett.*, vol. 117, no. 26, 2020, Art. no. 261103, doi: 10.1063/5.0033126.

[83] Z. Zhao et al., "Modal coupling and crosstalk due to turbulence and divergence on free space THz links using multiple orbital angular momentum beams," *Sci. Rep.*, vol. 11, no. 1, 2021, Art. no. 2110, doi: 10.1038/s41598-020-80179-3.

[84] X. Su et al., "Receiver aperture and multipath effects on power loss and modal crosstalk in a THz wireless link using orbital-angular-momentum multiplexing," *Sci. Rep.*, vol. 12, no. 1, 2022, Art. no. 14053, doi: 10.1038/s41598-022-18444-w.

[85] L. Ozyuzer et al., "Emission of coherent THz radiation from superconductors," *Science*, vol. 318, no. 5854, pp. 1291–1293, 2007, doi: 10.1126/science.1149802.

[86] S. Kalhor, S. Savel'ev, and K. Delfanazari, "Engineering ultrastrong coupling between Josephson plasmon polaritons and subwavelength microcavity arrays in silicon/van der Waals layered superconductor heterostructure for terahertz hybrid circuit cavity quantum electrodynamics," *Phys. Rev. B*, vol. 106, no. 24, 2022, Art. no. 245140, doi: 10.1103/PhysRevB.106.245140.

[87] P. Huang, T. Wang, R. Chen, P. Wang, Y. Zhou, and G. Zeng, "Experimental continuous-variable quantum key distribution using a thermal source," *New J. Phys.*, vol. 23, no. 11, 2021, Art. no. 113028, doi: 10.1088/1367-2630/ac3684.

[88] M. Zhang, P. Huang, P. Wang, S. Wei, and G. Zeng, "Experimental free-space continuous-variable quantum key distribution with thermal source," *Opt. Lett.*, vol. 48, no. 5, pp. 1184–1187, 2023, doi: 10.1364/OL.485166.